The CaFe Experiment:

Short-Range Pairing Mechanisms in Heavy Nuclei

Proposal to Jefferson Lab PAC 44

C.E. Hyde, M. Khachatryan, H. Szumila-Vance, L.B. Weinstein (co-spokesperson)
Old Dominion University, Norfolk VA

K. Allada, W. Bertozzi, S. Gilad, O. Hen (contact person), A Papadopoulou,
A. Schmidt, B.A. Schmookler, E.P. Segarra, and R. Cruz Torres
Massachusetts Institute of Technology, Cambridge, MA

E.O. Cohen (co-spokesperson), M. Duer, J. Lichtenstadt, E. Piasetzky, and O. Reich
Tel-Aviv University, Tel Aviv, Israel

J. Bericic, S.C. Dusa, S. Glamazdin, D.W. Higinbotham (co-spokesperson),
E. McClellan, D. Meekins, and B. Sawatsky
Thomas Jefferson National Accelerator Facility, Newport News, VA

J.R.M. Annand, D.J. Hamilton, and R. Montgomery
University of Glasgow, Scotland UK.

T. Brecelj, M. Mihovilovič, S. Širca, S. Štajner Jožef Stefan
Institute and University of Ljubljana, Slovenia

A. Beck, I. Korover, and S. Maytal-Beck
Nuclear Research Center Negev, Beer-Sheva, Israel

S. Wells, N. Simicevic, and R. Beminiwattha
Louisiana Tech University, Ruston, LA

M. Kohl, N. Kalantarians, A. Liyanage, B. Dongwi, J. Nazeer
Hampton University, Hampton, VA

P.E.C. Markowitz
Florida International University, Miami, FL

E. Long
University of New Hampshire, Durham, NH

K. Aniol
California State University, Los Angeles, CA

F. Benmokhtar
Duquesne University, Pittsburgh, PA

D. Androic
University of Zagreb, Bijenicka, Zagreb

S. Danagoulian
North Carolina A&T State University, Greensboro, NC

W. Tireman
Northern Michigan University, Marquette, MI

(Dated: June 5, 2016)

Abstract

Nucleon-nucleon short range correlated (NN SRC) pairs account for about 25% of nucleons in medium to heavy nuclei and about 75% of the nucleon's kinetic energy. Almost all high-momentum protons in nuclei have a correlated partner and that partner is almost always a neutron. While this general outline of nucleon pairing is explained by the nucleon-nucleon tensor force, we still do not understand quantitatively the details of the pairings. To learn more, we plan to systematically study how changing the number of protons and neutrons in a nucleus changes the probability of NN SRC pairings.

To do this, we will measure the $(e, e'p)$ reaction over a range of kinematics on several nuclei: d, ^{12}C, ^{40}Ca, ^{48}Ca, and ^{54}Fe. With this data, we will be able to determine the relative probability of finding high-momentum ($p > p_{fermi}$) and low momentum ($p < p_{fermi}$) protons in each nucleus. This will allow an experimental determination of how the pairing probability changes from the lightest symmetric nucleus, d, to ^{12}C, to a heavy symmetric nucleus ^{40}Ca; as well as determining the pairing probabilities with 8 more neutrons by going from ^{40}Ca to ^{48}Ca and then by adding 6 more protons going from ^{48}Ca to ^{54}Fe. The eight extra neutrons in ^{48}Ca compared to ^{40}Ca constitute a 40% increase in the neutron number. These eight neutrons are in the $1f_{7/2}$ shell, outside the ^{40}Ca closed shell, and are thus in very different orbitals from the protons they are expected to form pairs with.

The cross sections will be measured at high Q^2 and $x > 1$ to reduce the effects of Meson Exchange Currents and Isobar Currents and in non-perpendicular kinematics to reduce the effects of Final State Interactions. We will use 40 uA of 11 GeV beam in Hall-C and detect the scattered electrons in the SHMS and the knocked out protons in the HMS. We request four days of beamtime to significantly improve our quantitative understanding of nucleon pairing in nuclei.

I. INTRODUCTION AND MOTIVATION

A. Short Range Correlated NN Pairs in Nuclei

The mean field approximation describes bulk properties of nuclei such as shell structure, excitation energies, and spins remarkably well; however, only about 70% of nucleons occupy mean field orbitals [1, 2]. Describing the dynamics of the remaining nucleons is a major challenge facing nuclear physics today.

The Jefferson Lab 6 GeV program made tremendous progress in understanding these remaining nucleons. Results from inclusive (e, e') measurements at $x = Q^2/2m\nu > 1$ (see Section II B for variable definitions) indicate that the nucleon momentum distributions in all nuclei are remarkably similar for $p > 275$ MeV/c [3–5]. About 25% of nucleons in medium to heavy nuclei have momentum greater than the typical mean-field (Fermi) momentum, $p > p_{fermi}$ where $p_{fermi} \approx 250$ MeV/c [4, 5]. Exclusive $(e, e'pN)$ measurements show that in the symmetric ^{4}He and ^{12}C nuclei, almost every proton with momentum $300 < k < 600$ MeV/c has a correlated partner nucleon, with neutron-proton (np) pairs outnumbering proton-proton (pp) and, by inference, neutron-neutron (nn) pairs by a factor of ≈ 20 [6–8]. In asymmetric heavy nuclei with unequal numbers of the different fermions, high-momentum protons still disproportionately belong to np pairs [9]. The observed np-SRC dominance in heavy nuclei is a non-trivial result since in these heavy nuclei, nucleons from different shells could create $l \neq 0$ pp and nn pairs with non-zero spin that are also sensitive to the tensor part of the NN-interaction, thereby diminishing the observed np dominance observed in light nuclei. Two of these results were published in *Science* [6, 9].

The observed np-SRC pair dominance also implies that in heavy neutron-rich nuclei the high-momentum tail contains the same amount of neutrons and protons, leaving the excess neutrons to occupy low-momentum states (see Fig. 1). This leads to a possible inversion of momentum sharing between protons and neutrons where protons (i.e. the minority) have larger average momentum. This inversion should be universal for two-component Fermi systems with a short-range interaction between the different Fermions.

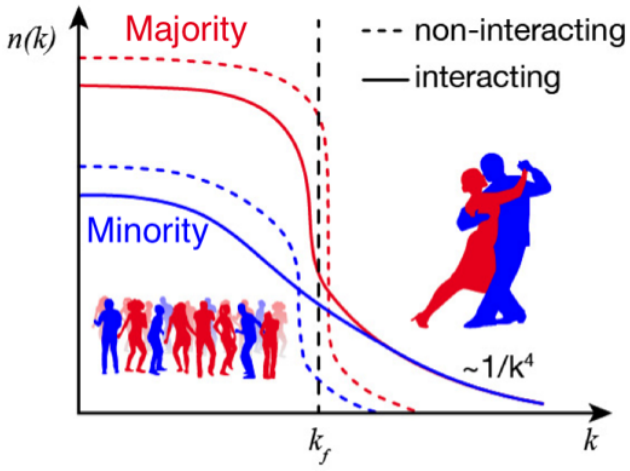

FIG. 1: A schematic representation of the main characteristics of the momentum distribution, $n(k)$, of asymmetric nuclei. The dashed lines show the standard non-interacting system while the solid lines show the effect of including a short-range interaction between different Fermions which creates a high-momentum ($k > k_F$) tail. This is analogous to a dance party with a majority of girls, where boy-girl interactions will make the average boy dance more than the average girl, and hence the boys will have larger average momentum [9].

B. Implications of momentum sharing in imbalanced Fermi systems

The *np*-dominance of SRC pairs and the resulting inversion of the momentum sharing in heavy neutron-rich imbalanced nuclei have wide ranging implications in astro, nuclear and particle physics. These include the determination of the density dependence of the nuclear symmetry-energy up to supra-nuclear densities [10–15], analysis of neutrino-nucleus scattering data for the determination of the nature of the electro-weak interaction [16, 17], the quark structure of bound nucleons through the EMC effect [18, 19], the isospin dependence of the EMC effect as a cause of the standard-model NuTeV anomaly [18, 20–23], double-beta decay matrix elements [24], neutron star equation of state and cooling rates [25], the universality of contact interactions in Fermi systems [26], etc.

1. Neutrino-nucleus scattering

One application of SRCs is in neutrino physics where most experiments still use a simple relativistic Fermi gas model to describe the nucleus. Recent high precision measurements of charged current quasi-elastic neutrino-nucleus scattering cross-sections [16, 17] show the need to include the effects of *np*-SRC pairs in both their reaction model and detector response.

This is expected to be a crucial ingredient in facilitating the precision requirements of next generation neutrino experiments, that require high precision measurements on neutrino and anti-neutrino interactions with asymmetric nuclei [27]. This proposed experiment will help us understand precisely which nucleons form SRC pairs, which in turn will improve our understanding of neutrino-nucleus interactions. In this way, these proposed measurements will complement experiment E12-14-012, which has been approved to extract the spectral function (i.e., the single-nucleon properties) of ^{40}Ar.

2. *The EMC effect and the NuTeV anomaly*

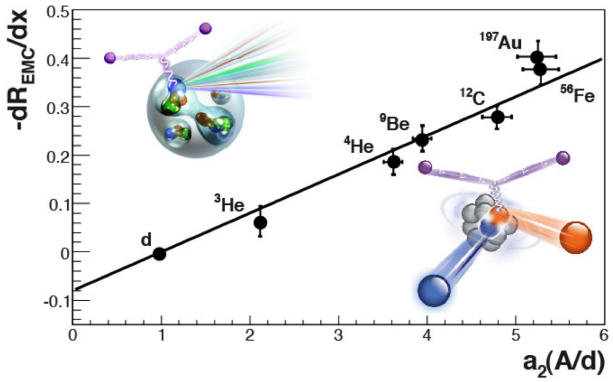

FIG. 2: The strength of the EMC effect plotted vs the relative probability of a nucleon to belong to an SRC pair for a variety of nuclei. See Refs. [18, 19] for details.

The deep inelastic scattering cross section for scattering from bound nucleons differs from that of free nucleons. This phenomenon, first discovered 30 years ago, is known as the EMC effect, and its origin is still not fully understood [28–32]. The EMC effect implies modification of bound nucleon structure [32] and its size is linearly correlated with the number of SRC (high momentum) pairs in nuclei (see Fig. 2) [18, 19]. This implies the possibility that both stem from high momentum (i.e., large virtuality) nucleons in the nucleus. Two 12-GeV experiments will measure deep inelastic scattering (DIS) off one nucleon in the deuteron by detecting (tagging) the high-momentum backward-angle spectator protons [33] or neutrons [34]. By measuring the nucleon-momentum dependence of the bound nucleon structure functions, these experiments will determine whether the EMC effect is due to a small modification of the large number of mean-field nucleons or a large modification of the smaller number of SRC nucleons.

Theoretical calculations show that an isospin dependent EMC effect in neutron-rich nuclei, and in particular iron, could explain the NuTeV anomaly [23]. The latter is a three

standard deviation difference from the Standard Model prediction in the measurement of the electroweak-mixing (Weinberg) angle using neutrino scattering from iron [22]. One original model employed a mean-field model to explain the possible existence of such an isospin dependent result. Alternatively, if the EMC nucleon modification is dominated by high momentum nucleons and protons have higher average momentum than neutrons in $N > Z$ nuclei, then this would provide an alternative model for an isospin dependent EMC effect which could quantitatively explain the NuTeV anomaly. By studying how changing the number of protons and neutrons affects the number of high momentum protons, our proposed measurement will provide input to calculations of the NuTeV anomaly.

3. The nuclear symmetry energy

The nuclear symmetry energy describes how the energy per nucleon in nuclear matter changes as a function of the proton fraction. While its value at the nuclear saturation density is relatively well constrained [14], its density dependence is not, largely due to uncertainties in the tensor component of the nucleon-nucleon interaction [12, 13]. Knowledge of this density dependence at supra-nuclear densities is important for different aspects of nuclear astrophysics and in particular neutron stars [14]. Recent calculations show that the inclusion of high-momentum tails, dominated by tensor force induced *np*-SRC pairs, dramatically softens the nuclear symmetry energy at supra-nuclear densities [10–13]. Including these high-momentum tails decreases the kinetic part of the nuclear symmetry energy at nuclear density from the free Fermi Gas Model value of +12.5 MeV to −10 MeV, increasing the potential part at saturation density and softening its density dependence [15]. Measuring the change in the average proton momentum (and hence, kinetic energy) as we change the number of neutrons and protons will help us refine this calculation.

4. Cooling rates of neutron stars

Theoretical analysis of neutrino cooling data indicates that neutron stars contain about 5 to 10% protons and electrons in the crust. Calculations show that *np*-dominance of SRC pairs in asymmetric nuclei and nuclear matter can bring a large fraction of the protons above their Fermi momentum, opening holes below the Fermi momentum. The existence of such

fast protons and the resulting holes in the Fermi sphere might allow for some direct, rather than modified, Urca cooling of neutron stars, even below threshold [25]. Since direct Urca cooling is about 10^6 times faster than modified Urca cooling, small changes could have a disproportionate impact on the cooling rate and the star lifetime.

New, high-precision data on the dynamics of 2N-SRC pairs in heavy nuclei and their dependence on the nuclear asymmetry will improve the accuracy and increase the reliability of such calculations.

5. *Ultra-cold interacting Fermi Systems*

Two-component many-body Fermi systems with a short-range interaction that is strong between different Fermions and weak between Fermions of the same type have several universal features [35] including the existence of a high-momentum tail ($k > k_F$) that scales as $n(k) = Ck^{-4}$ and is dominated by short-range correlated (SRC) pairs of different Fermions. The scale factor, C, is known as Tan's contact and describes the thermodynamics of the system.

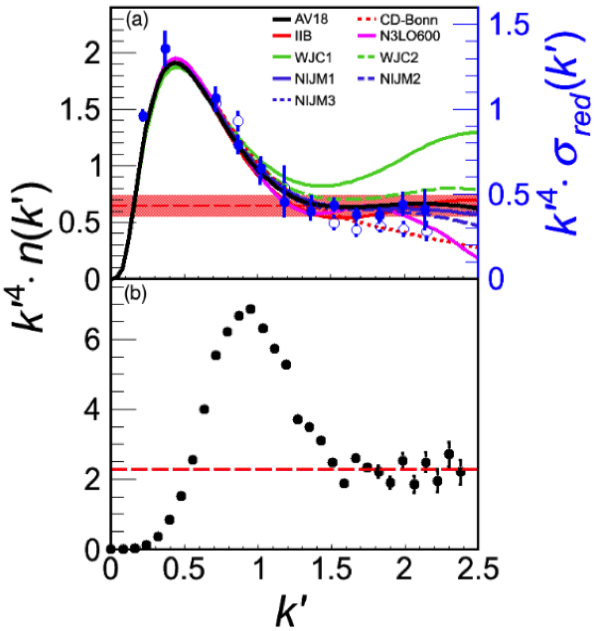

FIG. 3: The scaled momentum distribution, $k^4 n(k)$ in units of k_F, for nuclear (top) and atomic (bottom) systems. Bottom: The measured momentum distribution of ^{40}K atoms in a symmetric two-spin state ultra-cold gas with a short-range interaction between the different spin-states [36]. Top: The proton momentum distribution in deuterium calculated with state-of-the-art nucleon-nucleon potentials (solid lines) and the extracted from $d(e, e'p)$ cross-section measurements (blue points). The dashed lines are the results of a fit to a constant at $k > 1.5k_F$. See Ref. [26] for details.

The high-momentum tail and the thermodynamic Tan relations were experimentally verified in two-spin state ultra-cold atomic gases [36]. Fig. 3 shows the scaled momentum distribution, $k^4 n(k)$ in units of k_F, of ^{40}K atoms in ultra-cold balanced two-spin state atomic gas (bottom) [36] and of nucleons bound in deuterium (top) [26]. The deuteron momentum

distribution is calculated using state-of-the-art nucleon-nucleon potentials and extracted from $d(e, e'p)$ measurements. Both distributions have the same normalization for $n(k)$. The momentum distribution in both systems scales as k^{-4} starting at $k \approx 1.5k_F$ [26].

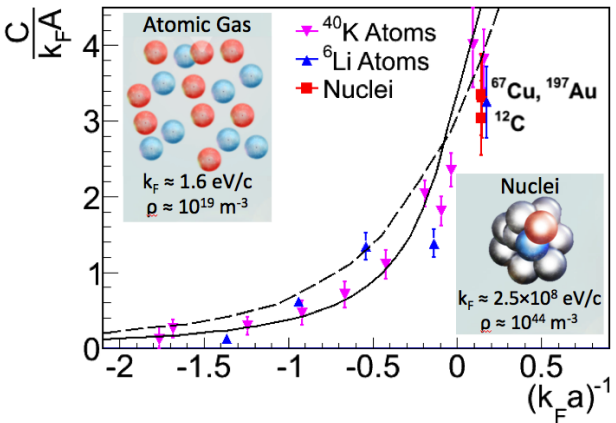

FIG. 4: The pairing probability, C, as a function of the dimensionless interaction strength for atomic and nuclear systems. See Ref. [26] for details.

Since the deuteron momentum distribution is proportional to k^{-4} and the nuclear momentum distributions at $k > 275$ MeV/c are proportional to the deuteron's [3–5], the momentum distribution for all nuclei scales as k^{-4} for $k > 275$ MeV/c. Fig. 4 shows the pairing probability, known as the Contact, for nuclear and atomic systems as a function of their dimensionless interaction strength. Despite at least a 20 order-of-magnitude difference in density, the atomic and nuclear systems have the same pairing probability for the same interaction strength.

A detailed study of the np-dominance of SRC pairs in heavy nuclei and its dependence on the nuclear asymmetry will allow a further study of the connection between Tan's universal relations, nuclei, and nuclear matter.

II. SHORT RANGE NUCLEON PAIRING MECHANISMS

We know from previous measurements that almost all high momentum nucleons in nuclei belong to SRC NN pairs and that these pairs are predominantly np pairs, even in heavy asymmetric nuclei such as lead. We also know that this unlike-fermion pairing is similar to pairing in two-component ultra-cold atomic gases. This pairing could also invert the average momentum in asymmetric nuclei, giving the minority nucleons more average momentum than the majority. However, we do not know the exact details of this pairing mechanism.

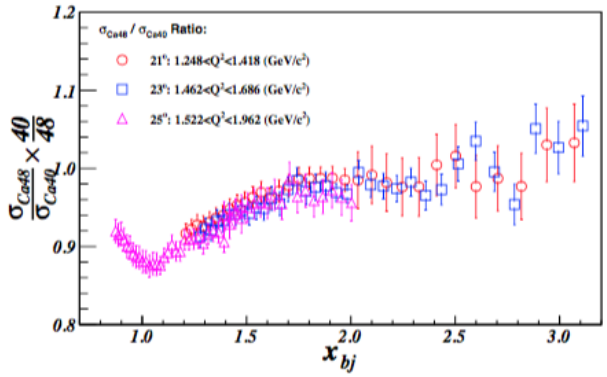

FIG. 5: The per-nucleon (e, e') cross section ratio of ^{48}Ca to ^{40}Ca. The ratio in the scaling region ($1.7 < x < 2$ for $Q^2 \approx 1.3$ and $1.5 < x < 2$ for $Q^2 \approx 2$ GeV^2) is about 0.97 [37].

E08-014 measured the per-nucleon ratio of (e, e') cross sections for ^{48}Ca to ^{40}Ca at $1.25 \leq Q^2 \leq 2$ GeV^2 [37]. If SRC is independent of isospin (i.e., due to all possible nn, np and pp pairs), then the cross section for scattering from one nucleon in an SRC pair is

$$\sigma \propto 2\sigma_{ep}(Z(Z-1)/2) + (\sigma_{ep} + \sigma_{en})(NZ) + 2\sigma_{en}(N(N-1)/2) \quad . \tag{1}$$

At the E08-014 measured momentum transfer, $\sigma_{ep} \approx 3\sigma_{en}$. Thus, for isospin independent SRC, the per-nucleon cross section ratio of ^{48}Ca to ^{40}Ca should be 1.10. On the other hand, if SRC are dominated by np pairs and we apply simple pair counting (e.g., NZ), then the expected ratio of ^{48}Ca to ^{40}Ca would be 1.17. These predictions are very similar and difficult to distinguish experimentally. However, the measured per-nucleon cross section ratio is about 0.97, disagreeing with both simple predictions (see Fig. 5). A more sophisticated calculation counting the number of NN pairs in a nodeless relative S-state [38–40] predicted a ratio of 0.99. This is discussed in more detail below.

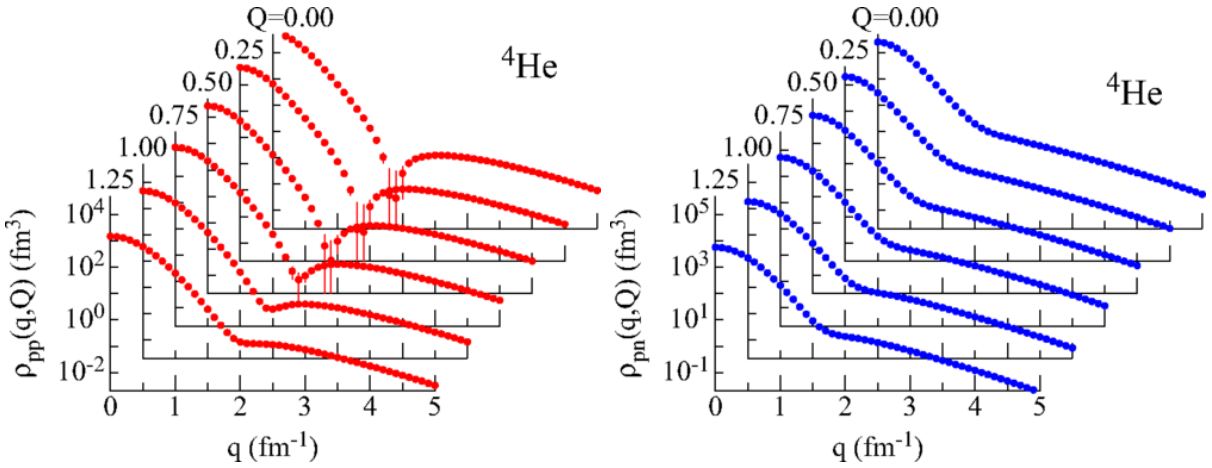

FIG. 6: The proton-proton (left) and proton-neutron (right) momentum distribution in ^{4}He averaged over the directions of the relative ($\vec{q}$) and total ($\vec{Q}$) pair momenta as a function of q for several fixed values of Q from 0 to 1.25 fm^{-1} [41].

Exact calculations of nuclear wave functions are only possible for relatively light nuclei, up to approximately ^{12}C [41]. They find that np pairs dominate at high relative momentum ($300 \leq p_{rel} \leq 600$ MeV/c) (see Fig. 6). Even in ^{8}He, where combinatorially there are more nn pairs than np pairs, the momentum density of the np pairs is greater than the nn pairs at $p_{rel} > 200$ MeV/c. This is one more example of the failure of simple pair-counting combinatorics.

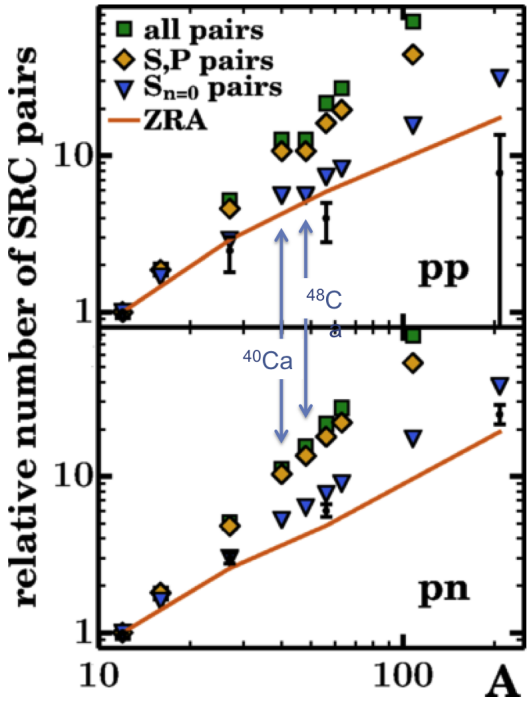

FIG. 7: Mass dependence of the number of pp (top panel) and pn (bottom panel) SRC pairs of nucleus A relative to ^{12}C . Data (small black circles with error bars) are extracted from the measured CLAS $A(e,e'p)$ and $A(e,e'pp)$ cross-section ratios [9, 21] after correcting for FSI. The green squares correspond with unconditional counting of the pp pairs ($Z(Z-1)/30$) and pn pairs ($ZN/36$) for ^{12}C, ^{16}O, ^{27}Al, ^{40}Ca, ^{48}Ca, ^{56}Fe, ^{63}Cu, ^{108}Ag, and ^{208}Pb. The yellow diamonds are the ratios obtained by counting independent particle model (IPM) pairs in relative S or P states. The blue triangles count IPM ($l = 0, n = 0$) pairs. The solid line denotes the result of a reaction-model calculation for scattering from close-proximity (zero-range) pairs which takes full account of the experimental phase space [42].

Ryckebusch, Cosyn and collaborators [40] have calculated single-nucleon momentum distributions in heavier nuclei by shifting the complexity induced by SRC from the wave functions to the operators. They find that the SRC-related high momentum tail of the single-nucleon momentum distribution is dominated by correlation operators acting on mean-field pairs with zero relative radial and angular momentum quantum numbers ($n = 0, l = 0$). Using this method, we calculated the expected number of NN SRC pairs in nuclei from carbon to lead and compared that to the experimentally extracted number of pn and pp pairs in those nuclei [38, 39, 42]. The measured number of pp and pn pairs increases far more slowly than simple combinatorics ($Z(Z-1)/2$ and NZ respectively) and is much more consistent with the number of NN pairs with $n = 0, l = 0$ (see Fig. 7) [42]. Note that the number of pp pairs is the same for ^{40}Ca and ^{48}Ca, while the number of pn pairs increases steadily from ^{40}Ca to ^{48}Ca to ^{56}Fe. This implies that adding neutrons to ^{40}Ca increases the number (and hence the proportion) of high momentum protons and that adding protons to ^{48}Ca increases the number, but not the proportion of high momentum protons.

A. Nucleon-nucleon pairing in nuclei

Since high-momentum protons in the nucleus almost entirely come from SRC NN pairs, we will use the number of detected high-momentum protons as a measure of the number of SRC pairs in a given nucleus. We expect these pairs to be predominantly np pairs.

We propose to measure the relative proportion of high-momentum protons in d, C, ^{40}Ca, ^{48}Ca, and ^{54}Fe to test short range pairing mechanisms. d, as the simplest nuclear system, will serve as a benchmark. C is a light symmetric nucleus that has already been studied in $(e, e'pN)$ reactions. ^{40}Ca and ^{48}Ca are both doubly closed-shell nuclei. ^{40}Ca has filled proton and neutron $1s, 1p$, and $2s/1d$ shells. ^{48}Ca has, in addition, eight more neutrons in the $1f_{7/2}$ shell. Somehow these extra $1f_{7/2}$ neutrons form SRC pairs with the 40 nucleons in the inner core. This pairing is non-trivial.

By measuring the relative number of high-momentum protons in C and ^{40}Ca, we can test how the number pN pairs changes from light to medium symmetric nuclei.

By measuring the relative number of high-momentum protons in ^{40}Ca and ^{48}Ca nuclei, we can directly measure the extra number of cross-shell np pairs caused by adding eight $1f_{7/2}$ neutrons.

Model	^{12}C	^{40}Ca	^{48}Ca	^{54}Fe	^{40}Ca/C	^{48}Ca/^{40}Ca	^{54}Fe/^{48}Ca	^{54}Fe/^{40}Ca
1 – all protons	12	20	20	26	1.7	1	1.3	1.3
2 – all pairs	234	2740	3380	4862	11.7	1.23	1.44	1.77
3 – all np pairs	36	400	560	728	10.1	1.4	1.30	1.82
4 – S and P np pairs	13.3	138.0	180.9	239.3	10.4	1.31	1.32	1.73
5 – $l = 0, n = 0$ np pairs	13.2	69.4	83.3	101.7	5.3	1.20	1.22	1.47

TABLE I: The expected number of high-momentum protons for each of the five models listed [42]. See text for description of models. The values for models 4 and 5 use ^{56}Fe rather ^{54}Fe. The absolute magnitude of the numbers in each row is arbitrary; only the ratios have any meaning.

Similarly, by adding six $1f_{7/2}$ protons to ^{48}Ca, we get ^{54}Fe. These extra protons can pair with any of the 40 nucleons in the inner shells or with the eight neutrons in the $1f_{7/2}$ shell. Thus, measuring the difference between ^{40}Ca and ^{48}Ca will teach us about the pairing of protons and neutrons from different shells and measuring the difference between ^{48}Ca and ^{54}Fe will teach us about the pairing of protons and neutrons from both different shells and the same shell.

We can predict the number of high momentum protons in the different nuclei in several different models:

1. isospin independence so that the the number of high momentum protons is proportional to the number of protons,

2. isospin-independent pair dominance with np, pp, and nn combinatorial pairs (see Eq. 1),

3. np pair dominance with combinatorial pairs (NZ),

4. np pair dominance with all relative S and P pairs [42] and

5. np pair dominance with only relative $n = 0, l = 0$ pairs [42].

The relative number of high-momentum protons for each of the five models is shown in Table I. Note that the normalizations of the different rows are very different so that only the ratios have any meaning.

The ratio of high-momentum protons in ^{40}Ca to C varies by a factor of two between the $l = 0, n = 0$ np pairs and less restrictive pair counting models. The ratio of high momentum protons in ^{48}Ca to ^{40}Ca varies by about 20%, and the ratio of high momentum protons in ^{54}Fe to ^{48}Ca varies by about 8%.

We will also compare ratios of the heavier nuclei to deuterium, as the simplest two body nuclear system.

B. Formalism

The cross section for electron-induced proton knockout from nuclei $A(e, e'p)$ can be written (assuming factorization) as:

$$\frac{d^6\sigma}{d\nu dE_{miss} d\Omega_e d\Omega_p} = K\sigma_{ep} S^D(E_{miss}, p_{miss})$$

where σ_{ep} is the cross section for scattering an electron from a bound proton, the missing energy and missing momentum are

$$E_{miss} = \nu - T_p - T_{A-1} \tag{2}$$

$$\vec{p}_{miss} = \vec{q} - \vec{p}_p \tag{3}$$

where T_p and T_{A-1} are the kinetic energies of the outgoing proton and residual nucleus, the momentum transfer $\vec{q} = \vec{p}_e - \vec{p}'_e$, $S^D(E_{miss}, p_{miss})$ is the distorted spectral function. and the kinematical factor K

$$K = \frac{E_p p_p}{(2\pi)^3}.$$

In the absence of final state interactions (FSI), S is the probability to find a nucleon in the nucleus with separation energy E_{miss} and momentum p_{miss} [43]. The energy transfer $\nu = E - E'$, E and E' are the initial and scattered electron energies, $\vec{p}_e$ and $\vec{p}'_e$ are the initial and scattered electron momenta, $\vec{p}_p$ is the outgoing proton momentum, and Ω_e and Ω_p are the electron and proton solid angles respectively. The angle between the recoil momentum ($\vec{p}_{recoil} = \vec{p}_{miss}$) and $\vec{q}$ is called θ_{rq}. We will restrict θ_{rq} to minimize final state interactions (see Section II C for details).

We plan to extract the distorted spectral function from the measured cross sections:

$$S^D(E_{miss}, p_{miss}) = \left(\frac{1}{K\sigma_{ep}}\right) \frac{d^6\sigma}{d\nu dE_{miss} d\Omega_e d\Omega_p} \tag{4}$$

and then correct it for the effects of FSI.

For each nucleus we plan to measure at one low-p_{miss} kinematics and one high-p_{miss} kinematics. We will correct the distorted spectral function for FSI. For each value of missing momentum we will only detect protons covering a fraction $f(p_{miss})$ of the 4π solid angle available to $\vec{p}_{miss}$. We will further correct our measurement by $1/f$ to account for this. We will then integrate the corrected distorted spectral functions over missing energy and missing momentum. The relative amount of high-momentum protons in each nucleus will equal the ratio of the integrated distorted spectral functions at high-p_{miss} and low-p_{miss}.

The double ratio of the integrated distorted spectral functions at high-p_{miss} and low-p_{miss} for different nuclei should correspond to the ratios in the last four columns of Table I.

The correction, $1/f$, for the undetected protons is purely geometrical. It is easy to calculate and will also cancel in the double ratio of high-p_{miss} and low-p_{miss} for different nuclei.

There are a number of uncertainties in the extraction of the distorted spectral function, including the validity of factorization, the off-shell extrapolation of the electron-proton cross section, and the effects of FSI. Over the limited acceptance of the spectrometers, factorization should be accurate to about 10% and the effects of factorization should cancel almost completely when calculating cross section ratios. Similarly, while there are several different off-shell prescriptions for the electron-proton cross section [44], the effects of these will also cancel when calculating ratios at similar p_{miss}. The effect of FSI is discussed in section II C.

C. Final State Interactions

We want to extract the

- ratios of high to low momentum protons in each of d, C, ^{40}Ca, ^{48}Ca, and ^{54}Fe,
- ratios of high-momentum protons in heavier nuclei to deuterium and in ^{40}Ca to C, ^{40}Ca to ^{48}Ca and in ^{54}Fe to ^{48}Ca, and
- double ratios of high to low momentum protons in heavier nuclei to deuterium, ^{40}Ca to C, ^{40}Ca relative to ^{48}Ca, and in ^{54}Fe relative to ^{48}Ca.

We will need to correct each of these ratios for the effects of final state interactions (FSI).

There are two general effects from rescattering of the outgoing proton: a shift in momentum due to the real part of the proton-nucleus potential, and rescattering of the proton that changes its momentum and potentially knocks out a second nucleon. Loss of protons from a particular kinematic bin can be calculated accurately in the Glauber approximation for high momentum protons. Rescattering of protons into a particular kinematic bin is harder to calculate.

We will measure the $(e, e'p)$ reaction at small angles between the momentum transfer and the recoil momentum, $\theta_{rq} \leq 40°$, to significantly reduce contributions from nucleon rescattering.

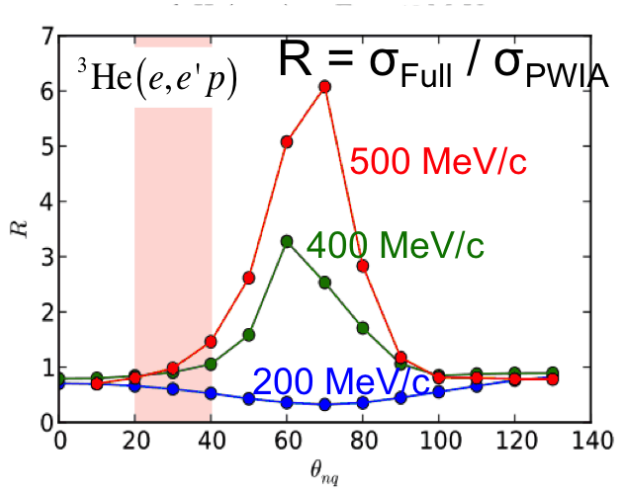

FIG. 8: The calculated ^{3}He$(e, e'p)$ ratio of the cross section which includes rescattering of the struck nucleon (FSI) to the PWIA cross section for $p_{miss} = 0.2$ (blue), 0.4 (green), and 0.5 (red) GeV/c as a function of θ_{rq}, the angle between the recoil momentum and $\vec{q}$ in the laboratory frame [45].

This rescattering of protons *into* a particular kinematic bin is maximum at perpendicular kinematics, where the angle between the recoil momentum and the momentum transfer, $\theta_{rq} \approx 70°$. This happens because most collisions between high-momentum protons and other nucleons in the nucleus deflect the high-momentum only slightly, kicking the struck nucleon out at about 70° (non-relativistically it would be about 90°). This can be seen clearly in calculations of the data of [46], where the cross section at $p_{miss} > 250$ MeV/c and $E_{miss} \approx p^2_{miss}/2m$ is due almost entirely to rescattering. Calculations by Sargsian [45] for ^{3}He$(e, e'p)$ show very large contributions due to proton rescattering peaked at $\theta_{rq} \approx 70°$. In order to avoid these regions where rescattering is much larger than the SRC signal, we will

choose $\theta_{rq} \leq 40°$.

We will calculate the rescattering of protons *out* of our kinematic bins using the Glauber approximation. Glauber calculations have been shown to reproduce nucleon transparency measurements in nuclei [47]. In addition, since we are primarily interested in the relative proportions of high- and low-initial-momentum protons in the different nuclei, we are primarily sensitive to the *difference* in the transparency from ^{40}Ca to ^{54}Fe. The measured transparency in ^{56}Fe at $Q^2 = 3.3$ GeV^2 is $T = 0.4$ [48]. The calculated transparency for knocked-out protons at $Q^2 = 2.4$ GeV^2 and $50 \leq p_{miss} \leq 150$ MeV/c (i.e., for kinematics similar to our proposed kinematics) is about $T = 0.43, 0.37$, and 0.36 for ^{40}Ca, ^{48}Ca, and ^{54}Fe, respectively. This difference is consistent with the expected variation of the opacity (equals one minus the transparency) as $A^{1/3}$.

For a given nucleus, protons with large and small p_{miss} have the same measured transparency [47]. Therefore the ratio of the large p_{miss} to small p_{miss} cross sections for a given nucleus should be independent of FSI.

The ratios of high-momentum protons in ^{40}Ca to ^{48}Ca and in ^{54}Fe to ^{48}Ca will need to be corrected for FSI. We will calculate the small change in the transparency from ^{54}Fe to ^{48}Ca and from ^{48}Ca to ^{40}Ca and compensate the data for it. In addition, we will construct an artificial, approximately $N = Z$ nucleus by averaging the results for ^{40}Ca and ^{54}Fe. Since the transparency of (^{40}Ca+^{54}Fe)/2 and ^{48}Ca should be very similar, the ratio of high momentum protons in (^{40}Ca + ^{54}Fe)/2 to ^{48}Ca should be almost independent of FSI.

D. Impact on the 12 GeV JLab program

The results of this proposed measurement will complement other 12 GeV JLab experiments, particularly measurements of the spectral function of ^{40}Ar, inclusive quasielastic (e, e') measurements of nuclei at $x > 1$, and inclusive deep inelastic (e, e') measurements of nuclei at $x < 1$ (EMC effect).

E12-14-012 will measure electro-induced proton knockout from ^{40}Ar (or possibly Ti) to extract its spectral function (i.e., its single-nucleon properties). They will measure the missing momentum distribution of the cross section for the different mean-field orbitals in argon ($1s_{1/2}, 2s_{1/2}, 1p_{1/2}, 1p_{3/2}, 1d_{3/2}$ and $1d_{5/2}$). Our measurement will focus instead on the knockout of high-momentum protons belonging to short range correlated pairs, studying

how their number changes when we change the number of neutrons and then the number of protons in the nucleus. Our measurement of SRC protons will thus complement E12-14-012's measurement of primarily mean-field protons.

E12-06-105 will measure inclusive electron scattering (e, e') on a wide variety of nuclei at $1.4 < x$ and $Q^2 \leq 5$ GeV^2 to extend previous studies of short range correlations in few-body and heavy nuclei. However, inclusive cross section measurements cannot distinguish between electron scattering from a proton or from a neutron and thus cannot distinguish between *pp* and *pn* SRC pairs. By studying how the number of high-momentum protons changes when we change the number of neutrons and then the number of protons in the nucleus, our experiment will provide complementary information.

E12-10-108 will measure the EMC effect in inclusive deep inelastic (e, e') measurements of nuclei at $x < 1$. By comparing their measurements of the EMC effect to the SRC ratios measured at $x > 1.4$ in E12-06-105, they will extend our understanding of the EMC-SRC correlation. By studying the details of proton-neutron pairing, our experiment will provide complementary information that will help us understand how the EMC effect and SRC ratios change from ^{40}Ca to ^{48}Ca.

Proposal PR12-14-007, "Constraints on Isovector-Dependent Nuclear Modification Effects Using Parity-Violating Deep Inelastic Scattering, seeks to measure the flavor-dependent nuclear medium modification (i.e., the EMC effect) in ^{48}Ca. The ^{48}Ca nucleus is chosen to maximize isospin asymmetry effects in a relatively well controlled nuclear environment. As mentioned, many models of the EMC effect relate medium modification of the bound nucleon structure to the virtuality of the nucleons in the nucleus, which is dominated by SRC nucleons. If in ^{48}CaSRC pairs are dominated by *np*-SRC pairs, protons will have larger probabality than neutrons to have high momentum which will naturally lead to an isospin dependent EMC effect. Observing the latter is the goal of PR12-14-007. This proposal and ours are complementary measurements that will shed light on the origin of the recent correlations between EMC and SRC pairs in nuclei and the isospin dependent EMC effect as an explanation to the NuTeV anomaly.

E. Previous Measurements

While there have been a number of $(e, e'p)$ experiments at Jefferson Lab [46, 48–59], they have almost all focused on measuring nuclear transparencies or single nucleon properties of nuclei (i.e., nucleon knockout from valence shells). Very few have measured $(e, e'p)$ at SRC kinematics. Some experiments focused on measuring the correlated partner of the knocked-out proton [6, 8, 60]. However, these experiments measured nucleon knockout from symmetric nuclei (He and C) and were thus insensitive to the effects on the proton momentum distribution of adding neutrons.

Both Rohe *et al* [57] and Benmokhtar *et al* [46] measured $(e, e'p)$ over a wide range of missing energy and missing momentum to look for the effects of correlations. Benmokhtar measured the ^{3}He$(e, e'p)$ cross section in perpendicular kinematics (where the missing momentum and hence the undetected nucleon is perpendicular to the momentum transfer) and thus their cross sections in the correlations region are dominated by nucleon rescattering. Rohe *et al.* extracted the nuclear spectral function as a function of E_{miss} for three different values of p_{miss} in parallel kinematics [57]. They compared the measured spectral function to calculations, finding reasonable agreement only at $p_{miss} \approx 250$ MeV/c. They were interested in observing the existence of the correlated part of the spectral function. Our experiment will study in detail how the correlated part changes from ^{40}Ca to ^{48}Ca to ^{54}Fe.

The overall proportion of high momentum nucleons in various nuclei has been extracted from per-nucleon ratios of $A(e, e')$ to $d(e, e')$ cross sections. This has been measured for nuclei from ^{3}He to Au. As shown in Fig. 5 and discussed in Sec. I A, the per-nucleon ratios of ^{48}Ca(e, e') to ^{40}Ca(e, e') cross sections is one. This measurement is sensitive to both high-momentum protons and neutrons in Ca. Our measurement will complement the inclusive (e, e') measurement, since it is only sensitive to protons.

This will be the first $(e, e'p)$ measurement at Jefferson Lab to investigate the effects on nucleon SRC pairing of adding a large number of neutrons and then a large number of protons in medium to heavy nuclei.

III. THE PROPOSED MEASUREMENT

We will measure the $(e, e'p)$ cross section on d, C, ^{40}Ca, ^{48}Ca, and ^{54}Fe at high and low missing momentum at large Q^2 and non-perpendicular kinematics. For the high p_{miss} kinematics we chose $Q^2 \approx 3.5$ GeV^2 to minimize the effects of Meson Exchange Currents and Isobar Configurations (Δ production). We chose $\theta_{rq} < 40^\circ$ to minimize the effects of Final State Interactions at large missing momentum. This reduces the energy transfer and thus gives $x = Q^2/2m\nu > 1$, also reducing the effects of MEC and IC.

We will extract the relative probability for a proton to be at high-p_{miss} ($p_{miss} > p_{Fermi} \approx$ 250 MeV/c) by calculating the ratio of the integrated cross section for high-p_{miss} to low-p_{miss} in each of the three nuclei. We will construct several ratios:

- single ratios of high to low momentum protons in each of d, C, ^{40}Ca, ^{48}Ca, and ^{54}Fe,
- single ratios of high-momentum protons in heavier nuclei to deuterium, ^{40}Ca to C, ^{40}Ca to ^{48}Ca and in ^{54}Fe to ^{48}Ca, and
- double ratios of high to low momentum protons in heavy nuclei relative to deuterium, ^{40}Ca relative to C, ^{40}Ca relative to ^{48}Ca, and in ^{54}Fe relative to ^{48}Ca.

The first and third ratios will be independent of FSI. The second will be corrected for the change in transparency among the various nuclei. Note that there is only a small change in transparency between ^{40}Ca and ^{54}Fe.

We will use an 11 GeV beam and measure the scattered electron in the SHMS and the knocked out proton in the HMS. The SHMS will operate at a scattering angle of 10°.

We will use the existing Jefferson Lab 0.5-cm thick, 0.93 g/cm^2 ^{48}Ca target, along with similar ^{40}Ca and ^{54}Fe targets. Both ^{40}Ca and ^{54}Fe target materials are readily available. The ^{40}Ca and ^{48}Ca targets can take at least 40 μA of beam; the C, ^{54}Fe and d targets can take up to 80 μA.

The proposed kinematics are shown in Table II.

A. From cross section to ratios

As described in Section II B, we will measure the $(e, e'p)$ cross section at high- and low-p_{miss} on d, C, ^{40}Ca, ^{48}Ca, and ^{54}Fe. We will extract the distorted spectral function using Eq.

TABLE II: Proposed kinematics and beam time for the measurement.

Q^2	$E_{\rm Beam}$	E'_e	θ_e	$\lvert\mathbf{p}_p\rvert$	θ_p	p_{miss}
GeV^2	GeV	GeV		GeV/c		GeV/c
3.5	11	9.85	10.0°	1.80	43.0°	0.45
3.5	11	9.85	10.0°	1.90	42.5°	0.15

4, correct it for the effects of FSI using the Glauber approximation [61], and correct it for the limited p_{miss}-dependent geometrical acceptance. We will then integrate the cross section over missing energy (up to π-emission threshold) and missing momentum. The low-p_{miss} bin will be integrated from 0 to 250 MeV/c and the high-p_{miss} bin will be integrated from about 350 to 550 MeV/c.

We will then construct the ratio of high-p_{miss} to the sum of low- and high-p_{miss} protons for each nucleus. These ratios will give the fraction of high momentum protons, and hence the protons belonging to SRC-pairs in each nucleus. We will compare these single-ratios to calculations of the proportions of high-momentum protons in the different nuclei. The effects of FSI should largely cancel in these ratios.

We will then construct the double ratios of high-p_{miss} to the sum of low- and high-p_{miss} protons for pairs of nuclei. The effects of FSI, ambiguities in the off-shell electron-proton cross section, and the geometrical extrapolation should all cancel in this double ratio. These double ratios should correspond to relative amounts of high-momentum protons in the last four columns of Table I.

B. Rate Estimates

To calculate the expected rates for this experiment at low-p_{miss} we used SIMC with spectral functions for the appropriate nuclei, scaled by their calculated transparencies. In the absence of realistic high-p_{miss} nuclear spectral functions for heavy nuclei, we estimated the high-p_{miss} rates for this experiment by extrapolating from a similar experiment at lower momentum transfer. We extrapolated the rates in two ways, first doing simple extrapolations using the luminosity, electron-proton cross section, and acceptance and second using the deuterium momentum distribution as a proxy for the high-p_{miss} distribution. At high

momenta the d, ^{12}C, ^{40}Ca, ^{48}Ca, and ^{54}Fe momentum distributions all have the same shape, and the per-nucleon magnitude was measured by Refs. [5, 37].

For our kinematics we ran SIMC in the following configuration:

1. electrons detected at the SHMS, protons at the HMS.
2. Beam dimensions $89 \times 42 \mu\text{m}^2$.
3. Collimator in place.
4. liquid "deuterium" target characteristics:
   (a) ^{40}Ca density 1.55 g/cm^3.
   (b) Target length 0.5 cm - areal density of 0.775 g/cm^2).
5. Total beam charge 1.152 C, equivalent to a single 8-hour shift with a beam current of 40 μA.
6. The proposed kinematical settings with $E_{\text{Beam}} = 11$ GeV (see Table II)

The following cuts were applied to select the events:

1. SHMS acceptance
   (a) $-0.04 < \theta(e') < 0.04$ rad,
   (b) $-0.024 < \phi(e') < 0.024$ rad,
   (c) $-0.1 < \delta(p_e)/p_e < 0.22$.
2. HMS acceptance
   (a) $-0.06 < \theta(p) < 0.06$ rad,
   (b) $-0.035 < \phi(p) < 0.035$ rad,
   (c) $-0.1 < \delta(p_p)/p_p < 0.1$.
3. $1.2 < x_B$
4. 0.35 GeV/c $< p_{miss}$
5. $\theta_{rq} < 50^\circ$.

1. *Low missing momentum kinematics*

For low missing momentum, the spectral functions for heavy nuclei exist, allowing SIMC to make reasonable rate estimates. Due to the large acceptance of the SHMS, low p_{miss} kinematics can also be measured with the same setting as the SHMS high p_{miss} kinematics, by relaxing the $x_B > 1$ and high-p_{miss} cuts. The HMS acceptance is somewhat more limited and thus requires a slightly different setting to maximize the acceptance (see Table II).

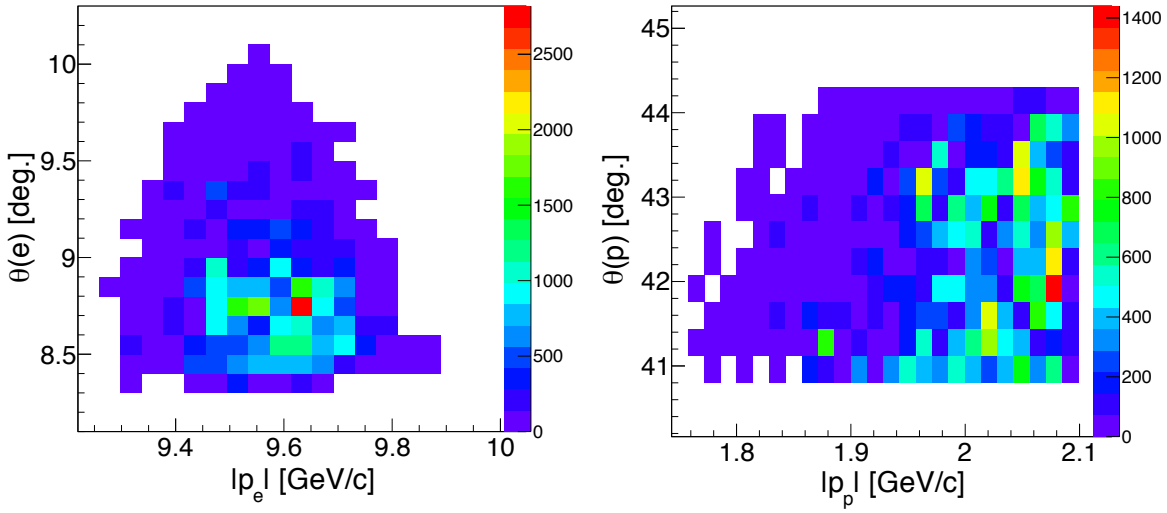

FIG. 9: The angle versus the momentum for (left) the electron detected in the SHMS and (right) ted in the HMS for low missing momentum kinematics with cuts as described in the text.

The simulation was performed using the standard SIMC ^{56}Fe mean-field spectral function with the same luminosity conditions, HMS and SHMS fiducial cuts, and a $p_{miss}<$ 250 MeV/c cut. As expected, the resulting event rate is extremely high, and exceeds 45,000 events/shift. See Figs. 9 and 10 for the predicted kinematic variables distributions.

2. *High missing momentum kinematics*

JLab experiment E01-015 ran in Hall-A and measured the ^{12}C$(e,e'p)$ reaction at $Q^2 = 2$ and $x_B = 1.2$, covering the same high missing momentum range of 350 – 550 MeV/c. We approximately extrapolated that measurement to this one as follows: We first scaled their event rate to the luminosity of this proposal, to get an event rate of 1920 events per shift. The Mott cross-section times the proton form factor squared decreased by a factor of about two,

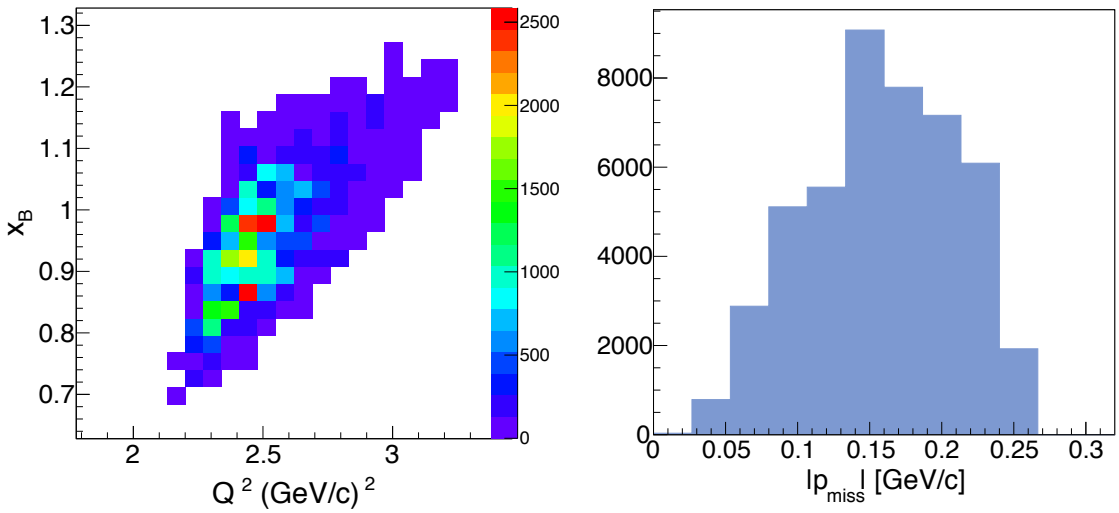

FIG. 10: On the left, the x_B scaling variable versus the momentum transfer, Q^2; and, on the right, the expected number of events versus missing momentum for the low missing momentum kinematics.

leading to an expected event rate of about 1000 events per shift. However, the considerably larger momentum acceptance of the Hall C spectrometers, combined with the kinematic focusing at higher Q^2, should increase the effective acceptance by about a factor of four, leading to a total of about 4000 events per shift.

We quantified this acceptance increase by performing SIMC simulations using the AV18 deuteron momentum distribution for the kinematics and acceptances of E01-015 and of this experiment.

We first verified this approach by performing SIMC simulations using the kinematics and acceptances of E01-015 and applying the same experimental cuts. The resulting simulated kinematical distributions matched the experimental ones, thus demonstrating the the applicability of using the deuteron momentum distribution for heavier nuclei.

We then ran SIMC for the kinematics and acceptances of this experiment. To get the expected number of high-p_{miss} ^{12}C events in this experiment, we scaled the measured number of events for E01-015 by the ratio of the number of simulated events for this experiment and E01-015. This scaling was consistent with the ballpark estimate described above. We then extrapolated from ^{12}C to ^{40}Ca, ^{48}Ca, and ^{54}Fe using the decrease in transparency from about 0.5 to about 0.4. The per-nucleon high-p_{miss} momentum distributions in the four nuclei should be within 20% of each other. The per-nucleon momentum distribution in

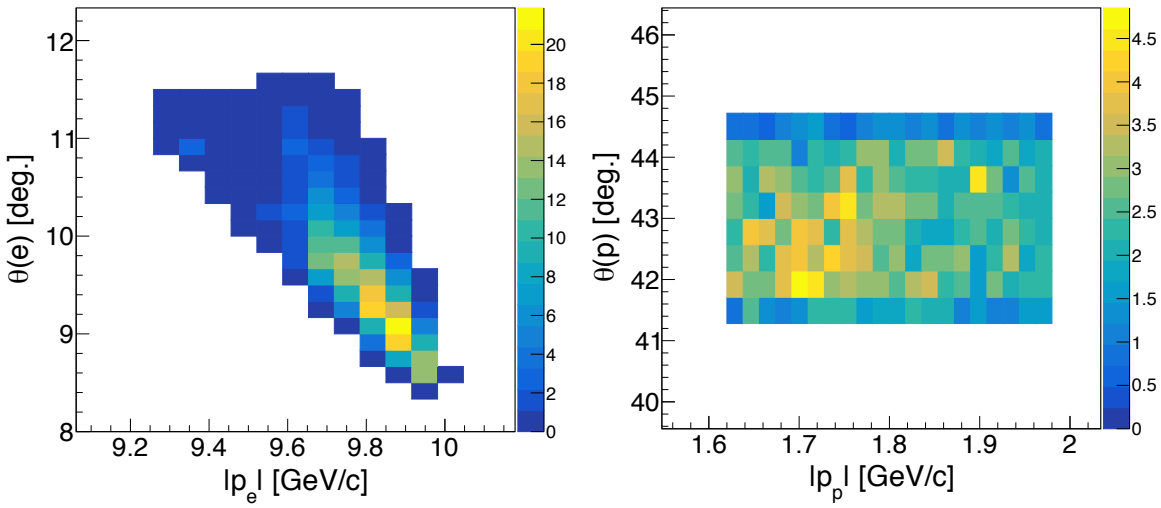

FIG. 11: The angle versus the momentum for (left) the electron detected in the SHMS and (right) the proton detected in the HMS with cuts as described in the text for the high-p_{miss} kinematics.

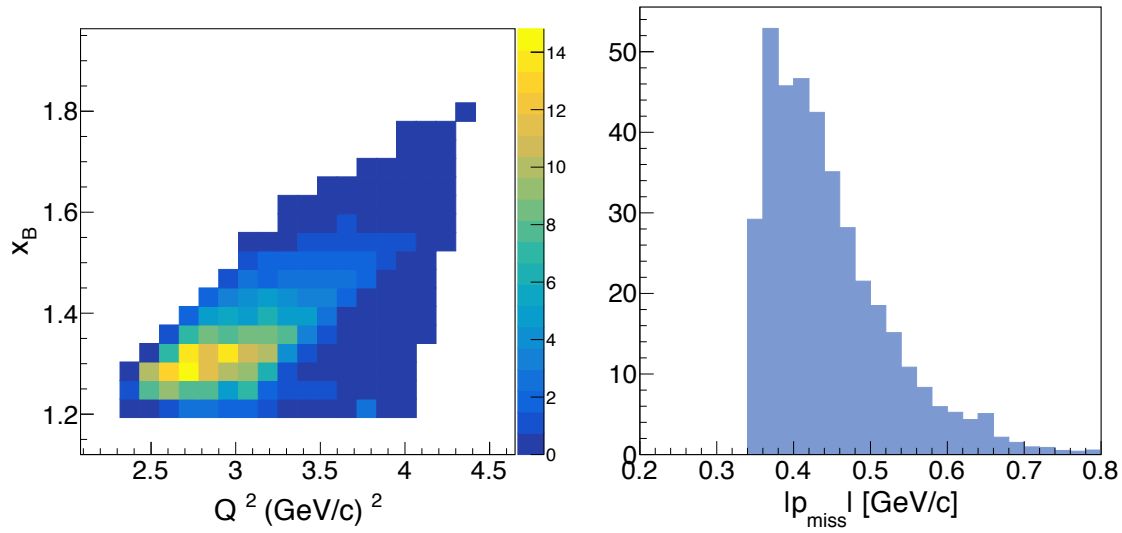

FIG. 12: On the left, the x_B scaling variable versus the momentum transfer, Q^2; and, on the right, the expected distribution of events versus missing momentum (the scale is arbitrary) for the high-p_{miss} kinematics with the cuts described in the text.

deuterium should be about four times smaller than that of C, but the losses transparency and radiative corrections will be much smaller.

The expected kinematical distributions after all cuts are shown in Figs. 11 and 12. Based on the cross section estimates, we expect to get several thousand events on each target for the high-p_{miss} kinematics.

This event rate will allow us to make very precise ($\approx 2\%$) measurements of the high-p_{miss} to low-p_{miss} ratio and to study the behavior of the ratio as a function of p_{miss}.

IV. BEAM TIME REQUEST AND EXPECTED RESULTS

This experiment requires 2 shifts for commissioning, calibrations and target changes, 2 shifts for the low-p_{miss} measurements on the five targets, and 8 shifts for the high-p_{miss} measurements on the five targets (as shown in Table III). Thus, we request a total of four days of beamtime in Hall-C using the HMS and SHMS in their standard configurations with 11 GeV beam and 40 μA on d, C, ^{40}Ca, ^{48}Ca, and ^{54}Fe targets. We will require a short period during the calibration time with a higher current, approximately 60 μA, for current calibrations and boiling tests.

TABLE III: requested beam time for each target in each kinematics.

kinematics	Target	Data-Taking [Hours]	Current [uA]	Expected Number of Events
high p_{miss}	^{2}H	12	40	4000
	^{12}C	10	40	4000
	^{40}Ca	14	40	4000
	^{48}Ca	14	40	4000
	^{54}Fe	14	40	4000
low p_{miss}	All Targets	16	40	10,000/Target
Commissioning and calibrations		12	20–60	
Target and Spectrometer Changes		4	N/A	
Total		96 (4 days)		

Based on similar experiments [62], we expect a $\approx$ 5% systematic uncertainty in the total cross section, including effects from acceptance corrections, radiative corrections, PID efficiency, charge measurement, target thickness, nuclear transparency etc. Most of these uncertainties will cancel when we construct ratios of cross sections. We conservatively expect that the remaining systematic uncertainties in the single ratios will be about 2–3% and the remaining systematic uncertainties in the double ratios (the ratio of high-$p_{miss}$to low-p_{miss}on one nucleus to that for a second nucleus) will be 1–2%.

The primary result of this measurement will be double ratios. We will construct the ratios of high-p_{miss} to the sum of low- and high-p_{miss} protons for each nucleus to determine

the relative probability of high-p_{miss} protons in each nucleus. We will then construct the ratio of the relative probability of high-p_{miss} protons in each nucleus relative to the other nuclei. The effects of FSI, ambiguities in the off-shell electron-proton cross section, and the geometrical extrapolation should all cancel in this double ratio. These double ratios should correspond to the relative amounts of high-momentum protons in the different nuclei in the last four columns of Table I.

We expect to measure the ratios of the relative amounts of high-momentum protons in the different nuclei to 2–3%. This will let us distinguish precisely among the different pairing models.

V. SUMMARY

We propose to increase our understanding of how protons pair in nuclei by measuring the proportion of high momentum protons in nuclei with dramatically different atomic weights, and dramatically different isospin.

We propose to measure the relative probability of finding high-momentum ($p > p_{fermi}$) and low momentum ($p < p_{fermi}$) protons in d, ^{12}C, ^{40}Ca, ^{48}Ca, and ^{54}Fe. Deuterium is the simplest nucleus and ^{12}C is the heaviest exactly calculable nucleus. We will measure how this probability changes from d, the simplest nucleus, to ^{12}C, a light symmetric nucleus, to ^{40}Ca, a heavier symmetric nucleus, as well as from ^{40}Ca to ^{48}Ca with 8 more neutrons, and then to ^{54}Fe, with 8 more neutrons and 6 more protons. The eight extra neutrons in ^{48}Ca constitute a 40% increase in the neutron number. These eight neutrons are in the $1f_{7/2}$ shell, outside the ^{40}Ca closed shell, and are thus in very different orbitals from the protons they are expected to pair with.

We will measure $A(e, e'p)$ cross sections and extract the probabilities of finding high and low missing-momentum protons from these cross sections. We will measure these cross sections at high Q^2 and $x > 1$ to reduce the effects of Meson Exchange Currents and Isobar Currents, and at non-perpendicular kinematics to reduce the effects of Final State Interactions. We will use an 11 GeV beam and detect the scattered electron in the SHMS and the knocked out proton in the HMS.

The double ratios of high and low missing momentum protons in different nuclei will correspond to the relative probabilities for protons to belong to SRC pairs in those nuclei. We will compare these double ratios to different models of proton pairing.

This measure will significantly improve our quantitative understanding of nucleon pairing in nuclei.

We request four days of 11 GeV beam time in Hall C for the measurements of d, ^{12}C, ^{40}Ca, ^{48}Ca, and ^{54}Fe$(e, e'p)$.

[1] L. Lapikas, Nuclear Physics A **553**, 293c (1993).

[2] G. Kramer, H. Blok, and L. Lapiks, Nuclear Physics A **679**, 267 (2001), ISSN 0375-9474, URL http://www.sciencedirect.com/science/article/pii/S0375947400003791.

[3] K. Egiyan et al. (CLAS Collaboration), Phys. Rev. C **68**, 014313 (2003).

[4] K. Egiyan et al. (CLAS Collaboration), Phys. Rev. Lett. **96**, 082501 (2006).

[5] N. Fomin et al., Phys. Rev. Lett. **108**, 092502 (2012).

[6] R. Subedi et al., Science **320**, 1476 (2008).

[7] E. Piasetzky, M. Sargsian, L. Frankfurt, M. Strikman, and J. W. Watson, Phys. Rev. Lett. **97**, 162504 (2006).

[8] I. Korover, N. Muangma, O. Hen, et al., Phys.Rev.Lett. **113**, 022501 (2014), 1401.6138.

[9] O. Hen et al. (CLAS Collaboration), Science **346**, 614 (2014).

[10] A. Carbone, A. Polls, and A. Rios, Euro. Phys. Lett. **97**, 22001 (2012).

[11] I. Vidaña, A. Polls, and C. m. c. Providência, Phys. Rev. C **84**, 062801 (2011), URL http://link.aps.org/doi/10.1103/PhysRevC.84.062801.

[12] C. Xu, A. Li, and B. Li, J. of Phys: Conference Series **420**, 012190 (2013).

[13] C. Xu and B. Li (2011), 1104:2075.

[14] J. M. Lattimer and Y. Lim, Apj **771**, 51 (2013).

[15] O. Hen, B.-A. Li, W.-J. Guo, L. B. Weinstein, and E. Piasetzky, Phys. Rev. C **91**, 025803 (2015), URL http://link.aps.org/doi/10.1103/PhysRevC.91.025803.

[16] G. A. Fiorentini et al. (MINERvA Collaboration), Phys. Rev. Lett. **111**, 022501 (2013).

[17] G. A. Fiorentini et al. (MINERvA Collaboration), Phys. Rev. Lett. **111**, 022502 (2013).

[18] L. B. Weinstein, E. Piasetzky, D. W. Higinbotham, J. Gomez, O. Hen, and R. Shneor, Phys. Rev. Lett. **106**, 052301 (2011).

[19] O. Hen, E. Piasetzky, and L. B. Weinstein, Phys. Rev. C **85**, 047301 (2012).

[20] L. Frankfurt and M. Strikman, Phys. Rep. **160**, 235 (1988).

[21] O. Hen et al., Int. J. Mod. Phys. E **22**, 133017 (2013).

[22] G. P. Zeller et al., **88**, 091802 (2002).

[23] I. C. Cloët, W. Bentz, and A. W. Thomas, Phys. Rev. Lett. **102**, 252301 (2009), URL http://link.aps.org/doi/10.1103/PhysRevLett.102.252301.

[24] F. Šimkovic, A. Faessler, H. Müther, V. Rodin, and M. Stauf, Phys. Rev. C **79**, 055501 (2009), URL http://link.aps.org/doi/10.1103/PhysRevC.79.055501.

[25] L. Frankfurt, M. Sargsian, and M. Strikman, International Journal of Modern Physics A **23**, 2991 (2008), http://www.worldscientific.com/doi/pdf/10.1142/S0217751X08041207, URL http://www.worldscientific.com/doi/abs/10.1142/S0217751X08041207.

[26] O. Hen, L. B. Weinstein, E. Piasetzky, G. A. Miller, M. M. Sargsian, and Y. Sagi, Phys. Rev. C **92**, 045205 (2015), URL http://link.aps.org/doi/10.1103/PhysRevC.92.045205.

[27] *"int workshop, neutrino-nucleus interactions for current and next generation neutrino oscillation experiments (int-13-54w).".*

[28] D. Geesaman, K. Saito, and A. Thomas, Ann. Rev. Nucl. and Part. Sci. **45**, 337 (1995).

[29] P. R. Norton, Rep. Prog. Phys. **66**, 1253 (2003).

[30] L. Frankfurt and M. Strikman, Phys. Rev. C **82**, 065203 (2010).

[31] S. A. Kulagin and R. Petti, Nucl. Phys. A **765**, 126 (2006).

[32] S. A. Kulagin and R. Petti, Phys. Rev. C **82**, 054614 (2010).

[33] O. Hen, L. Weinstein, S. Wood, and S. Gilad, *In Medium Nucleon Structure Functions, SRC, and the EMC effect, Jefferson Lab experiment E12-11-107* (2011).

[34] O. Hen, L. Weinstein, E. Piasetzky, and H. Hakobyan, *In Medium Proton Structure Functions, SRC, and the EMC effect, Jefferson Lab experiment E12-11-003A* (2015).

[35] E. Braaten, in *The BCS-BEC Crossover and the Unitary Fermi Gas*, edited by W. Zwerger (Springer, Berlin, 2012).

[36] J. T. Stewart, J. P. Gaebler, T. E. Drake, and D. S. Jin, Phys. Rev. Lett. **104**, 235301 (2010).

[37] Z. Ye, Ph.D. thesis, University of Virginia (2013), 1408.5861.

[38] M. Vanhalst, W. Cosyn, and J. Ryckebusch, Phys. Rev. C **84**, 031302 (2011), URL http://link.aps.org/doi/10.1103/PhysRevC.84.031302.

[39] M. Vanhalst, J. Ryckebusch, and W. Cosyn, Phys. Rev. C **86**, 044619 (2012).

[40] J. Ryckebusch, M. Vanhalst, and W. Cosyn, Journal of Physics G: Nuclear and Particle Physics **42**, 055104 (2015), 1405.3814, URL http://stacks.iop.org/0954-3899/42/i=5/a=055104.

[41] R. B. Wiringa, R. Schiavilla, S. C. Pieper, and J. Carlson, Phys. Rev. C **89**, 024305 (2014).

[42] C. Colle, O. Hen, W. Cosyn, I. Korover, E. Piasetzky, J. Ryckebusch, and L. B. Weinstein, Phys. Rev. C **92**, 024604 (2015).

[43] J. Kelly, Adv. Nucl. Phys. **23**, 75 (1996).

[44] T. De Forest, Nucl. Phys. **A392**, 232 (1983).

[45] M. Sargsian, *Private communication*.

[46] F. Benmokhtar et al. (Jefferson Lab Hall A Collaboration), Phys. Rev. Lett. **94**, 082305 (2005).

[47] O. Hen et al. (CLAS Collaboration), Phys.Lett. **B722**, 63 (2013), 1212.5343.

[48] K. Garrow, D. McKee, A. Ahmidouch, C. S. Armstrong, J. Arrington, R. Asaturyan, S. Avery, O. K. Baker, D. H. Beck, H. P. Blok, et al., Phys. Rev. C **66**, 044613 (2002), URL http://link.aps.org/doi/10.1103/PhysRevC.66.044613.

[49] K. Fissum et al. (Jefferson Lab Hall A Collaboration), Phys.Rev. **C70**, 034606 (2004), nucl-ex/0401021.

[50] J. Gao et al., Phys. Rev. Lett. **84**, 3265 (2000).

[51] N. Liyanage, B. D. Anderson, K. A. Aniol, L. Auerbach, F. T. Baker, J. Berthot, W. Bertozzi, P.-Y. Bertin, L. Bimbot, W. U. Boeglin, et al. (The Jefferson Lab Hall A Collaboration), Phys. Rev. Lett. **86**, 5670 (2001), URL http://link.aps.org/doi/10.1103/PhysRevLett.86.5670.

[52] J. Herraiz, Ph.D. thesis, Universidad Complutense de Madrid (2010).

[53] D. Dutta et al., Phys. Rev. C **68**, 064603 (2003), URL http://link.aps.org/doi/10.1103/PhysRevC.68.064603.

[54] J. Arrington, D. Higinbotham, G. Rosner, and M. Sargsian, Prog.Part.Nucl.Phys. **67**, 898 (2012), 1104.1196.

[55] M. M. Rvachev et al. (Jefferson Lab Hall A Collaboration), Phys. Rev. Lett. **94**, 192302 (2005).

[56] D. Rohe, O. Benhar, C. S. Armstrong, R. Asaturyan, O. K. Baker, S. Bueltmann, C. Carasco, D. Day, R. Ent, H. C. Fenker, et al. (E97-006 Collaboration), Phys. Rev. C **72**, 054602 (2005), URL http://link.aps.org/doi/10.1103/PhysRevC.72.054602.

[57] D. Rohe, C. S. Armstrong, R. Asaturyan, O. K. Baker, S. Bueltmann, C. Carasco, D. Day, R. Ent, H. C. Fenker, K. Garrow, et al. (E97-006 Collaboration), Phys. Rev. Lett. **93**, 182501 (2004), URL http://link.aps.org/doi/10.1103/PhysRevLett.93.182501.

[58] O. Hen, H. Hakobyan, R. Shneor, E. Piasetzky, L. Weinstein, W. Brooks, S. M.-T. Beck, S. Gilad, I. Korover, A. Beck, et al., Physics Letters B **722**, 63 (2013), ISSN 0370-2693, URL http://www.sciencedirect.com/science/article/pii/S0370269313002906.

[59] P. Monaghan, R. Shneor, R. Subedi, B. D. Anderson, K. Aniol, J. Annand, J. Arrington,

H. B. Benaoum, F. Benmokhtar, P. Bertin, et al., Journal of Physics G: Nuclear and Particle Physics **41**, 105109 (2014), URL http://stacks.iop.org/0954-3899/41/i=10/a=105109.

[60] R. Shneor et al., Phys. Rev. Lett. **99**, 072501 (2007).

[61] C. Colle, W. Cosyn, and J. Ryckebusch, *Final-state interactions in two-nucleon knockout reactions* (2015), 1512.07841.

[62] D. Dutta and R. Ent, *The Search for Color Transparency at 12 GeV, Jefferson Lab Experiment E12-06-107* (2006).

REPORTS

NUCLEAR PHYSICS

Momentum sharing in imbalanced Fermi systems

O. Hen,[1]* M. Sargsian,[2] L. B. Weinstein,[3] E. Piasetzky,[1] H. Hakobyan,[4,5] D. W. Higinbotham,[6] M. Braverman,[1] W. K. Brooks,[4] S. Gilad,[7] K. P. Adhikari,[3] J. Arrington,[8] G. Asryan,[5] H. Avakian,[6] J. Ball,[9] N. A. Baltzell,[8] M. Battaglieri,[10] A. Beck,[1,11] S. May-Tal Beck,[1,11] I. Bedlinskiy,[12] W. Bertozzi,[7] A. Biselli,[13] V. D. Burkert,[6] T. Cao,[14] D. S. Carman,[6] A. Celentano,[10] S. Chandavar,[15] L. Colaneri,[16] P. L. Cole,[6,17,18] V. Crede,[19] A. D'Angelo,[16,20] R. De Vita,[10] A. Deur,[6] C. Djalali,[14,21] D. Doughty,[6,22] M. Dugger,[23] R. Dupre,[24] H. Egiyan,[6] A. El Alaoui,[8] L. El Fassi,[3] L. Elouadrhiri,[6] G. Fedotov,[14,25] S. Fegan,[10] T. Forest,[17] B. Garillon,[24] M. Garcon,[9] N. Gevorgyan,[5] Y. Ghandilyan,[5] G. P. Gilfoyle,[26] F. X. Girod,[6] J. T. Goetz,[15] R. W. Gothe,[14] K. A. Griffioen,[27] M. Guidal,[24] L. Guo,[2,6] K. Hafidi,[8] C. Hanretty,[28] M. Hattawy,[24] K. Hicks,[15] M. Holtrop,[29] C. E. Hyde,[3] Y. Ilieva,[14,30] D. G. Ireland,[31] B. I. Ishkanov,[25] E. L. Isupov,[25] H. Jiang,[14] H. S. Jo,[24] K. Joo,[32] D. Keller,[28] M. Khandaker,[17,33] A. Kim,[34] W. Kim,[34] F. J. Klein,[18] S. Koirala,[3] I. Korover,[1] S. E. Kuhn,[3] V. Kubarovsky,[6] P. Lenisa,[35] W. I. Levine,[36] K. Livingston,[31] M. Lowry,[6] H. Y. Lu,[14] I. J. D. MacGregor,[31] N. Markov,[32] M. Mayer,[3] B. McKinnon,[31] T. Mineeva,[32] V. Mokeev,[6,24,37] A. Movsisyan,[35] C. Munoz Camacho,[24] B. Mustapha,[8] P. Nadel-Turonski,[6] S. Niccolai,[24] G. Niculescu,[38] I. Niculescu,[38] M. Osipenko,[10] L. L. Pappalardo,[35,39] R. Paremuzyan,[5,29] K. Park,[6,34] E. Pasyuk,[6] W. Phelps,[2] S. Pisano,[40] O. Pogorelko,[12] J. W. Price,[41] S. Procureur,[9] Y. Prok,[3,28] D. Protopopescu,[31] A. J. R. Puckett,[32] D. Rimal,[2] M. Ripani,[10] B. G. Ritchie,[23] A. Rizzo,[16] G. Rosner,[31] P. Roy,[19] P. Rossi,[6] F. Sabatié,[9] D. Schott,[30] R. A. Schumacher,[36] Y. G. Sharabian,[6] G. D. Smith,[42] R. Shneor,[1] D. Sokhan,[31] S. S. Stepanyan,[34] S. Stepanyan,[6] P. Stoler,[43] S. Strauch,[14,30] V. Sytnik,[4] M. Taiuti,[44] S. Tkachenko,[28] M. Ungaro,[6] A. V. Vlassov,[12] E. Voutier,[45] N. K. Walford,[18] X. Wei,[6] M. H. Wood,[14,46] S. A. Wood,[6] N. Zachariou,[14] L. Zana,[29,42] Z. W. Zhao,[28] X. Zheng,[28] I. Zonta,[16] Jefferson Lab CLAS Collaboration†

The atomic nucleus is composed of two different kinds of fermions: protons and neutrons. If the protons and neutrons did not interact, the Pauli exclusion principle would force the majority of fermions (usually neutrons) to have a higher average momentum. Our high-energy electron-scattering measurements using ^{12}C, ^{27}Al, ^{56}Fe, and ^{208}Pb targets show that even in heavy, neutron-rich nuclei, short-range interactions between the fermions form correlated high-momentum neutron-proton pairs. Thus, in neutron-rich nuclei, protons have a greater probability than neutrons to have momentum greater than the Fermi momentum. This finding has implications ranging from nuclear few-body systems to neutron stars and may also be observable experimentally in two-spin–state, ultracold atomic gas systems.

Many-body systems composed of interacting fermions are common in nature, ranging from high-temperature superconductors and Fermi liquids to atomic nuclei, quark matter, and neutron stars. Particularly intriguing are systems that include a short-range interaction that is strong between unlike fermions and weak between the same type of fermions. Recent theoretical advances show that even though the underlying interaction can be very different, these systems share several universal features (*1*–*4*). In all of these systems, this interaction creates short-range–correlated (SRC) pairs of unlike fermions with a large relative momentum ($k_{rel} > k_F$) and a small center-of-mass momentum ($k_{tot} < k_F$), where k_F is the Fermi momentum of the system. This pushes fermions from low momenta ($k < k_F$, where k is the fermion momentum) to high momenta ($k > k_F$), creating a "high-momentum tail."

In atomic nuclei, SRC pairs have been studied using many different reactions, including pick-up, stripping, and electron and proton scattering. The results of these studies highlighted the importance of correlations in nuclei, which lead to a high-momentum tail and decreased occupancy of low-lying nuclear states (*5*–*13*).

Recent experimental studies of balanced (symmetric) interacting Fermi systems, with an equal number of fermions of the two kinds, confirmed these predictions of a high-momentum tail populated almost exclusively by pairs of unlike fermions (*8*–*11*, *14*–*16*). These experiments were carried out using very different Fermi systems: protons and neutrons in atomic nuclei and two-spin–state, ultracold atomic gases. These systems span more than 15 orders of magnitude in Fermi energy from 10^6 to 10^{-9} eV and exhibit different short-range interactions [predominantly a strong tensor interaction in the nuclear systems (*8*, *9*, *17*, *18*) and a tunable Feshbach resonance in the atomic system (*14*, *15*)]. For cold atoms, Tan (*1*–*3*) showed that the momentum density decreases as C/k^4 for large k. The scale factor, C, is known as Tan's contact and describes many properties of the system (*4*). Similar pairing of nucleons in nuclei with $k > k_F$ was also predicted in (*19*).

In this work, we extend these previous studies to imbalanced (asymmetric) nuclear systems, with unequal numbers of the different fermions. When there is no interaction, the Pauli exclusion principle pushes the majority fermions (usually neutrons) to a higher average momentum. Including a short-range interaction introduces a new universal feature: the probability for a fermion to have momentum $k > k_F$ is greater for the minority than for the majority fermions. This is because the short-range interaction populates the high-momentum

[1]Tel Aviv University, Tel Aviv 69978, Israel. [2]Florida International University, Miami, FL 33199, USA. [3]Old Dominion University, Norfolk, VA 23529, USA. [4]Universidad Técnica Federico Santa María, Casilla 110-V Valparaíso, Chile. [5]Yerevan Physics Institute, 375036 Yerevan, Armenia. [6]Thomas Jefferson National Accelerator Facility, Newport News, VA 23606, USA. [7]Massachusetts Institute of Technology, Cambridge, MA 02139, USA. [8]Argonne National Laboratory, Argonne, IL 60439, USA. [9]Commissariat à l'Energie Atomique et aux Energies Alternatives, Centre de Saclay, Irfu/Service de Physique Nucléaire, 91191 Gif-sur-Yvette, France. [10]Istituto Nazionale di Fisica Nucleare (INFN), Sezione di Genova, 16146 Genova, Italy. [11]Nuclear Research Center Negev, P.O. Box 9001, Beer-Sheva 84190, Israel. [12]Institute of Theoretical and Experimental Physics, Moscow, 117259, Russia. [13]Fairfield University, Fairfield, CT 06824, USA. [14]University of South Carolina, Columbia, SC 29208, USA. [15]Ohio University, Athens, OH 45701, USA. [16]INFN, Sezione di Roma Tor Vergata, 00133 Rome, Italy. [17]Idaho State University, Pocatello, ID 83209, USA. [18]Catholic University of America, Washington, DC 20064, USA. [19]Florida State University, Tallahassee, FL 32306, USA. [20]Università di Roma Tor Vergata, 00133 Rome, Italy. [21]University of Iowa, Iowa City, IA 52242, USA. [22]Christopher Newport University, Newport News, VA 23606, USA. [23]Arizona State University, Tempe, AZ 85287-1504, USA. [24]Institut de Physique Nucléaire ORSAY, Orsay, France. [25]Skobeltsyn Institute of Nuclear Physics, Lomonosov, Russia. [26]University of Richmond, Richmond, VA 23173, USA. [27]College of William and Mary, Williamsburg, VA 23187-8795, USA. [28]University of Virginia, Charlottesville, VA 22901, USA. [29]University of New Hampshire, Durham, NH 03824-3568, USA. [30]The George Washington University, Washington, DC 20052, USA. [31]University of Glasgow, Glasgow G12 8QQ, UK. [32]University of Connecticut, Storrs, CT 06269, USA. [33]Norfolk State University, Norfolk, VA 23504, USA. [34]Kyungpook National University, Daegu 702-701, Republic of Korea. [35]INFN, Sezione di Ferrara, 44100 Ferrara, Italy. [36]Carnegie Mellon University, Pittsburgh, PA 15213, USA. [37]Moscow State University, Moscow, 119234, Russia. [38]James Madison University, Harrisonburg, VA 22807, USA. [39]Universitá di Ferrara, 44122 Ferrara, Italy. [40]INFN, Laboratori Nazionali di Frascati, 00044 Frascati, Italy. [41]California State University, Dominguez Hills, Carson, CA 90747, USA. [42]Edinburgh University, Edinburgh EH9 3JZ, UK. [43]Rensselaer Polytechnic Institute, Troy, NY 12180-3590, USA. [44]Università di Genova, 16146 Genova, Italy. [45]Laboratoire de Physique Subatomique et de Cosmologie, Universite Joseph Fourier, CNRS/IN2P3, Institut National Polytechnique, Grenoble, France. [46]Canisius College, Buffalo, NY 14208, USA.

***Corresponding author. E-mail: or.chen@mail.huji.ac.il** †The collaboration on this paper consists of all listed authors. There are no additional collaborators.

tail with equal numbers of majority and minority fermions, thereby leaving a larger fraction of majority fermions in low-momentum states ($k < k_F$) (see Fig. 1). In neutron-rich nuclei, this increases the average proton momentum and may even result in protons having higher average momentum than neutrons, inverting the momentum sharing in imbalanced nuclei from that in noninteracting systems. Theoretically, this can happen because of the tensor part of the nucleon-nucleon interaction, which creates predominantly spin-1, isospin-0 neutron-proton (np) SRC pairs (*17*, *18*).

Here we identify SRC pairs in the high-momentum tail of nuclei heavier than carbon with more neutrons (N) than protons (Z) (i.e., $N > Z$). The data show the universal nature of SRC pairs, which even in lead (N/Z = 126/82) are still predominantly np pairs. This np-pair dominance causes a greater fraction of protons than neutrons to have high momentum in neutron-rich nuclei.

The data presented here were collected in 2004 in Hall B of the Thomas Jefferson National Accelerator Facility using a 5.014-GeV electron beam incident on ^{12}C, ^{27}Al, ^{56}Fe, and ^{208}Pb targets. We measured electron-induced two-proton knockout reactions (Fig. 2). The CEBAF Large Acceptance Spectrometer (CLAS) (*20*) was used to detect the scattered electron and emitted protons. CLAS uses a toroidal magnetic field and six independent sets of drift chambers, time-of-flight scintillation counters, Cerenkov counters, and electromagnetic calorimeters for charged-particle identification and trajectory reconstruction (Fig. 2) (*16*).

We selected events in which the electron interacts with a single fast proton from an SRC pair in the nucleus (*9*, *16*) by requiring a large four-momentum transfer $Q^2 = \vec{q}^{\,2} - (\omega/c)^2 > 1.5$ GeV$^2/c^2$ [where $\vec{q}$ and ω are the three-momentum and energy, respectively, transferred to the nucleus and c is the speed of light] and Bjorken scaling parameter $x_B = Q^2/(2m_N \cdot \omega) > 1.2$ (where m_N is the nucleon mass). To ensure selection of events in which the knocked-out proton belonged to an SRC pair, we further required missing momentum $300 < |\vec{p}_{miss}| < 600$ MeV/c, where $\vec{p}_{miss} = \vec{p}_p - \vec{q}$ with $\vec{p}_p$ the measured proton momentum. We suppressed contributions from inelastic excitations of the struck nucleon by limiting the reconstructed missing mass of the two-nucleon system $m_{miss} < 1.1$ GeV/c^2. In each event, the leading proton that absorbed the transferred momentum was identified by requiring that its momentum $\vec{p}_p$ is within 25° of $\vec{q}$ and that $|\vec{p}_p|/|\vec{q}| \geq 0.6$ (*16*, *21*).

When a second proton was detected with momentum greater than 350 MeV/c, it was emitted almost diametrically opposite to $\vec{p}_{miss}$ (see fig. S19). The observed backward-peaked angular distributions are very similar for all four measured

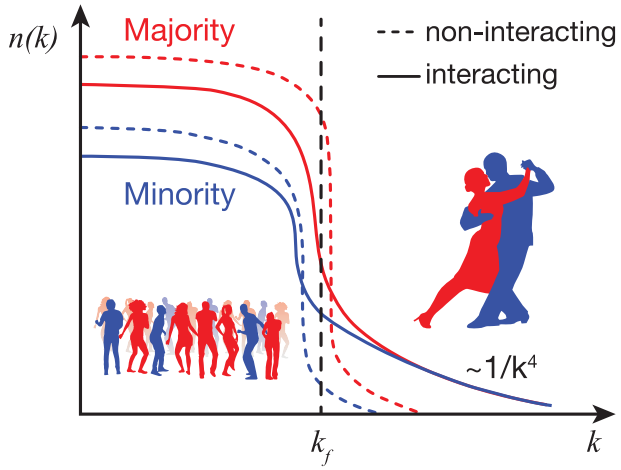

Fig. 1. Schematic representation of the momentum distribution, *n*(*k*), of two-component imbalanced Fermi systems. Red and blue dashed lines show the noninteracting system, whereas the solid lines show the effect of including a short-range interaction between different fermions. Such interactions create a high-momentum tail ($k > k_F$, where k_F is the Fermi momentum of the system). This is analogous to a dance party with a majority of girls, where boy-girl interactions will make the average boy dance more than the average girl.

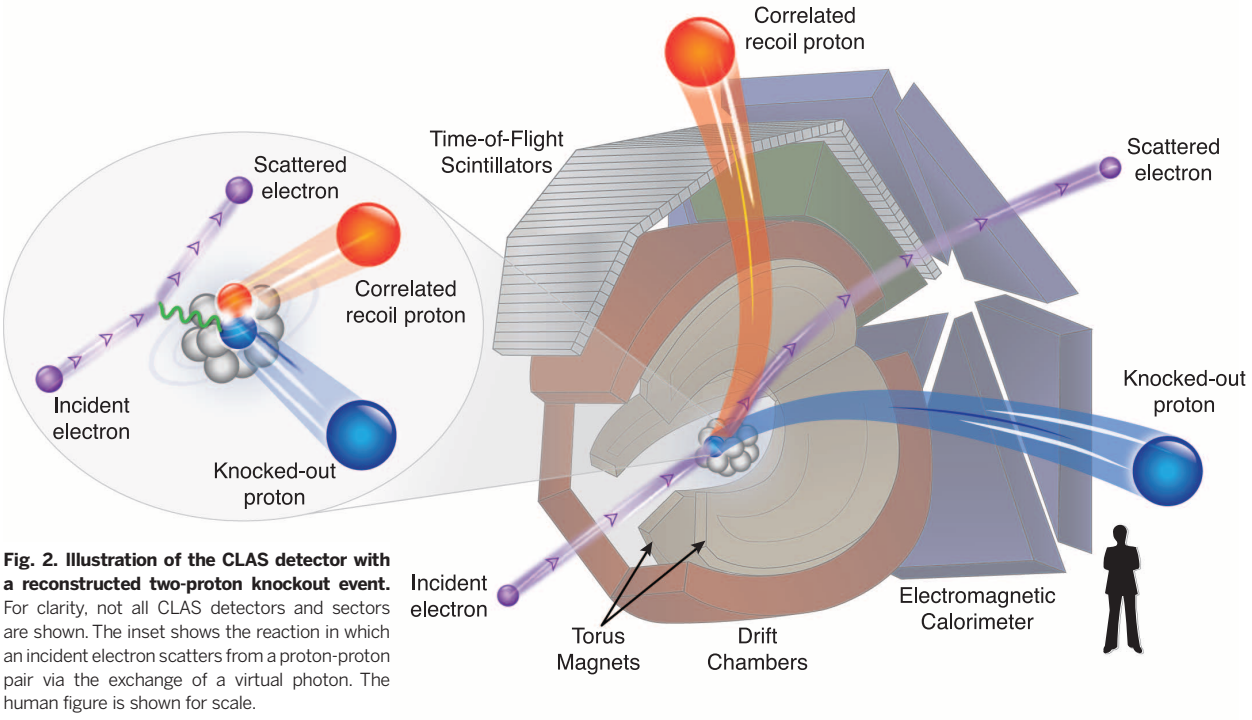

Fig. 2. Illustration of the CLAS detector with a reconstructed two-proton knockout event. For clarity, not all CLAS detectors and sectors are shown. The inset shows the reaction in which an incident electron scatters from a proton-proton pair via the exchange of a virtual photon. The human figure is shown for scale.

nuclei. This backward peak is a strong signature of SRC pairs, indicating that the two emitted protons were largely back-to-back in the initial state, having a large relative momentum and a small center-of-mass momentum (*8*, *9*). This is a direct observation of proton-proton (pp) SRC pairs in a nucleus heavier than ^{12}C.

Electron scattering from high–missing-momentum protons is dominated by scattering from protons in SRC pairs (*9*). The measured single-proton knockout ($e,e'p$) cross section (where e denotes the incoming electron, e' the measured scattered electron, and p the measured knocked-out proton) is sensitive to the number of pp and np SRC pairs in the nucleus, whereas the two-proton knockout ($e,e'pp$) cross section is only sensitive to the number of pp-SRC pairs. Very few of the single-proton knockout events also contained a second proton; therefore, there are very few pp pairs, and the knocked-out protons predominantly originated from np pairs.

To quantify this, we extracted the $[A(e,e'pp)/A(e,e'p)]/[^{12}C(e,e'pp)/^{12}C(e,e'p)]$ cross-section double ratio for nucleus A relative to ^{12}C. The double ratio is sensitive to the ratio of np-to-pp SRC pairs in the two nuclei (*16*). Previous measurements have shown that in ^{12}C nearly every high-momentum proton ($k > 300$ MeV/$c > k_F$) has a correlated partner nucleon, with np pairs outnumbering pp pairs by a factor of ~20 (*8*, *9*).

To estimate the effects of final-state interactions (reinteraction of the outgoing nucleons in the nucleus), we calculated attenuation factors for the outgoing protons and the probability of the electron scattering from a neutron in an np pair, followed by a neutron-proton single-charge exchange (SCX) reaction leading to two outgoing protons. These correction factors are calculated as in (*9*) using the Glauber approximation (*22*) with effective cross sections that reproduce previously measured proton transparencies (*23*), and using the measured SCX cross section of (*24*). We extracted the cross-section ratios and deduced the relative pair fractions from the measured yields following (*21*); see (*16*) for details.

Figure 3 shows the extracted fractions of np and pp SRC pairs from the sum of pp and np pairs in nuclei, including all statistical, systematic, and model uncertainties. Our measurements are not sensitive to neutron-neutron SRC pairs. However, by a simple combinatoric argument, even in ^{208}Pb these would be only $(N/Z)^2 \sim 2$ times the number of pp pairs. Thus, np-SRC pairs dominate in all measured nuclei, including neutron-rich imbalanced ones.

The observed dominance of np-over-pp pairs implies that even in heavy nuclei, SRC pairs are dominantly in a spin-triplet state (spin 1, isospin 0), a consequence of the tensor part of the nucleon-nucleon interaction (*17*, *18*). It also implies that there are as many high-momentum protons as neutrons (Fig. 1) so that the fraction of protons above the Fermi momentum is greater than that of neutrons in neutron-rich nuclei (*25*).

In light imbalanced nuclei ($A \leq 12$), variational Monte Carlo calculations (*26*) show that this results in a greater average momentum for the minority component (see table S1). The minority component can also have a greater average momentum in heavy nuclei if the Fermi momenta of protons and neutrons are not too dissimilar. For heavy nuclei, an np-dominance toy model that quantitatively describes the features of the momentum distribution shown in Fig. 1 shows that in imbalanced nuclei, the average proton kinetic energy is greater than that of the neutron, up to ~20% in ^{208}Pb (*16*).

The observed np-dominance of SRC pairs in heavy imbalanced nuclei may have wide-ranging implications. Neutrino scattering from two nucleon currents and SRC pairs is important for the analysis of neutrino-nucleus reactions, which are used to study the nature of the electro-weak interaction (*27*–*29*). In particle physics, the distribution of quarks in these high-momentum nucleons in SRC pairs might be modified from that of free nucleons (*30*, *31*). Because each proton has a greater probability to be in a SRC pair than a neutron and the proton has two u quarks for each d quark, the u-quark distribution modification could be greater than that of the d quarks (*19*, *30*). This could explain the difference between the weak mixing angle measured on an iron target by the NuTeV experiment and that of the Standard Model of particle physics (*32*–*34*).

In astrophysics, the nuclear symmetry energy is important for various systems, including neutron stars, the neutronization of matter in core-collapse supernovae, and r-process nucleosynthesis (*35*). The decomposition of the symmetry energy at saturation density ($\rho_0 \approx 0.17$ fm^{-3}, the maximum density of normal nuclei) into its kinetic and potential parts and its value at supranuclear densities ($\rho > \rho_0$) are not well constrained, largely because of the uncertainties in the tensor component of the nucleon-nucleon interaction (*36*–*39*). Although at supranuclear densities other effects are relevant, the inclusion of high-momentum tails, dominated by tensor-force–induced np-SRC pairs, can notably soften the nuclear symmetry energy (*36*–*39*). Our measurements of np-SRC pair dominance in heavy imbalanced nuclei can help constrain the nuclear aspects of these calculations at saturation density.

Based on our results in the nuclear system, we suggest extending the previous measurements of Tan's contact in balanced ultracold atomic gases to imbalanced systems in which the number of atoms in the two spin states is different. The large experimental flexibility of these systems will allow observing dependence of the momentum-sharing inversion on the asymmetry, density, and strength of the short-range interaction.

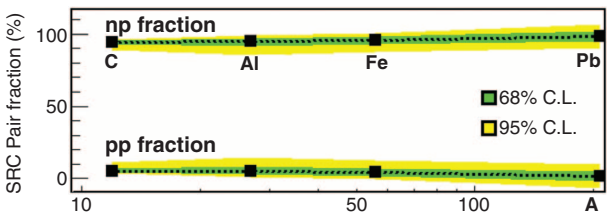

Fig. 3. The extracted fractions of np (top) and pp (bottom) SRC pairs from the sum of pp and np pairs in nuclei. The green and yellow bands reflect 68 and 95% confidence levels (CLs), respectively (*9*). np-SRC pairs dominate over pp-SRC pairs in all measured nuclei.

ACKNOWLEDGMENTS

This work was supported by the U.S. Department of Energy (DOE) and the National Science Foundation, the Israel Science Foundation, the Chilean Comisión Nacional de Investigación Científica y Tecnológica, the French Centre National de la

REFERENCES AND NOTES

1. S. Tan, *Ann. Phys.* **323**, 2952–2970 (2008).
2. S. Tan, *Ann. Phys.* **323**, 2971–2986 (2008).
3. S. Tan, *Ann. Phys.* **323**, 2987–2990 (2008).
4. E. Braaten, in *Lecture Notes in Physics* (Springer, Berlin, 2012), vol. 836, p. 193.
5. L. Lapikás, *Nucl. Phys. A.* **553**, 297–308 (1993).
6. K. I. Blomqvist *et al*., *Phys. Lett. B* **421**, 71–78 (1998).
7. R. Starink *et al*., *Phys. Lett. B* **474**, 33–40 (2000).
8. E. Piasetzky, M. Sargsian, L. Frankfurt, M. Strikman, J. W. Watson, *Phys. Rev. Lett.* **97**, 162504 (2006).
9. R. Subedi *et al*., *Science* **320**, 1476–1478 (2008).
10. K. Sh. Egiyan *et al*., *Phys. Rev. Lett.* **96**, 082501 (2006).
11. N. Fomin *et al*., *Phys. Rev. Lett.* **108**, 092502 (2012).
12. V. R. Pandharipande, I. Sick, P. K. A. deWitt Huberts, *Rev. Mod. Phys.* **69**, 981–991 (1997).
13. J. Arrington, D. W. Higinbotham, G. Rosner, M. Sargsian, *Prog. Part. Nucl. Phys.* **67**, 898–938 (2012).
14. J. T. Stewart, J. P. Gaebler, T. E. Drake, D. S. Jin, *Phys. Rev. Lett.* **104**, 235301 (2010).
15. E. D. Kuhnle *et al*., *Phys. Rev. Lett.* **105**, 070402 (2010).
16. Materials and methods are available as supplementary materials on *Science* Online.
17. R. Schiavilla, R. B. Wiringa, S. C. Pieper, J. Carlson, *Phys. Rev. Lett.* **98**, 132501 (2007).
18. M. M. Sargsian, T. V. Abrahamyan, M. I. Strikman, L. L. Frankfurt, *Phys. Rev. C* **71**, 044615 (2005).
19. L. Frankfurt, M. Strikman, *Phys. Rep.* **160**, 235–427 (1988).
20. B. A. Mecking *et al*., *Nucl. Inst. Meth. A* **503**, 513–553 (2003).
21. O. Hen *et al*., *Phys. Lett. B* **722**, 63–68 (2013).
22. I. Mardor, Y. Mardor, E. Piasetsky, J. Alster, M. M. Sargsyan, *Phys. Rev. C* **46**, 761–767 (1992).
23. D. Dutta, K. Hafidi, M. Strikman, *Prog. Part. Nucl. Phys.* **69**, 1–27 (2013).
24. J. L. Friedes, H. Palevsky, R. Stearns, R. Sutter, *Phys. Rev. Lett.* **15**, 38–41 (1965).
25. M. M. Sargsian, *Phys. Rev. C* **89**, 034305 (2014).
26. R. B. Wiringa, R. Schiavilla, S. C. Pieper, J. Carlson, *Phys. Rev. C* **89**, 024305 (2014).
27. L. Fields *et al*., *Phys. Rev. Lett.* **111**, 022501 (2013).
28. G. A. Fiorentini *et al*., *Phys. Rev. Lett.* **111**, 022502 (2013).
29. Neutrino-Nucleus Interactions for Current and Next Generation Neutrino Oscillation Experiments, Institute for Nuclear Theory (INT) workshop INT-13-54W, University of Washington, Seattle, WA, 3 to 13 December 2013.
30. O. Hen, D. W. Higinbotham, G. A. Miller, E. Piasetzky, L. B. Weinstein, *Int. J. Mod. Phys. E* **22**, 133017 (2013).
31. L. B. Weinstein *et al*., *Phys. Rev. Lett.* **106**, 052301 (2011).
32. G. P. Zeller *et al*., *Phys. Rev. Lett.* **88**, 091802 (2002).
33. G. P. Zeller *et al*., *Phys. Rev. Lett.* **90**, 239902 (2003).
34. I. C. Cloët, W. Bentz, A. W. Thomas, *Phys. Rev. Lett.* **102**, 252301 (2009).
35. J. M. Lattimer, Y. Lim, *Astrophys. J.* **771**, 51 (2013).
36. A. Carbone, A. Polls, A. Rios, *Europhys. Lett.* **97**, 22001 (2012).
37. I. Vidana, A. Polls, C. Providencia, *Phys. Rev. C* **84**, 062801(R) (2011).
38. C. Xu, A. Li, B. A. Li, *J. Phys. Conf. Ser.* **420**, 012090 (2013).
39. B.-A. Li, L.-W. Chen, C. M. Ko, *Phys. Rep.* **464**, 113–281 (2008).

Recherche Scientifique and Commissariat a l'Energie Atomique, the French-American Cultural Exchange, the Italian Istituto Nazionale di Fisica Nucleare, the National Research Foundation of Korea, and the UK's Science and Technology Facilities Council. Jefferson Science Associates operates the Thomas Jefferson National Accelerator Facility for the DOE, Office of Science, Office of Nuclear Physics under contract DE-AC05-06OR23177. The raw data from this experiment are archived in Jefferson Lab's mass storage silo.

SUPPLEMENTARY MATERIALS

www.sciencemag.org/content/346/6209/614/suppl/DC1
Materials and Methods
Figs. S1 to S30
Tables S1 to S8
References (*40*–*51*)

2 June 2014; accepted 2 October 2014
Published online 16 October 2014;
10.1126/science.1256785